Available online at www.sciencedirect.com
ScienceDirect
Geochimica et Cosmochimica Acta 71 (2007) 1159–1169
Geochimica
www.elsevier.com/locate/gca

Experimental study of D/H isotopic fractionation factor of water adsorbed on porous silica tubes

Thierry Richard *, Lionel Mercury, Marc Massault, Jean-Luc Michelot

UMR-CNRS 8148 "IDES", Université Paris-Sud, Bât. 504, 91405 Orsay, France

Received 10 April 2006; accepted in revised form 28 November 2006

Abstract

This paper presents D/H isotopic fractionation factor measurements of water adsorbed on porous silica tubes in isotopic equilibrium with water vapor. The fractionation factor is measured as a function of vapor pressure ranging from 10% to 80% RH (relative humidity) at room temperature. It is shown that the fractionation factor between the adsorption film or nanometrically confined water and vapor is smaller than that between bulk liquid water and vapor. A qualitative analysis relates this deuterium depletion to a modification of the zero-point energy of the water isomers in the adsorbed/confined state. Furthermore, the behavior of the fractionation factor with RH shows two different linear trends. The transition between the two (at 60% RH) may indicate the transition from a two-dimensional adsorbed water to a three-dimensional water network.

1. Introduction

The structure and properties of adsorbed and confined water are of specific interest in geochemical studies. Water–rock interactions and diffusion of dissolved species are at least partly controlled by the water activity which changes either in a under-saturated environment (e.g., Seshadri et al., 2001; Uchida et al., 2002; Benavente et al., 2004), or under the surface forces field of a confining solid (e.g., Bogdan, 2002; Santiso et al., 2005; Shirinyan et al., 2005). These two types of situation have in common that they are controlled by the properties of thin adsorbed films or confined water in thin pores. And these properties result from a specific combination of the solid and liquid properties, difficult to calculate directly.

Good examples of natural porous media with small pore sizes are argillaceous rocks that are studied as potential candidates for deep nuclear-waste storage. Their hydraulic conductivity is very low (for instance, $<10^{-14}$ m s^{-1} in the Tournemire argillite, Boisson et al., 2001) and diffusion is therefore considered as the main mode of transport for dissolved species. To obtain information on the natural diffusive transfers in these media, numerous recent studies used the stable isotope composition of pore water, and particularly the spatial distribution of deuterium contents, at the scale of the clay formations (Rübel et al., 2002; Hendry et al., 2004; Patriarche et al., 2004). The isotopic composition of water bound to the solid phase is obviously an important issue in such studies, for both data acquisition and interpretation. Some authors (e.g., Rübel and Bath, 2002) assumed that bound water should be enriched in heavy isotopes with respect to bulk water. However, this more or less "intuitive" consideration is not supported by experimental studies (Stewart, 1972; Araguás-Araguás et al., 1995; Karlsson, 2001). These experiments, which pointed towards a D-depleted adsorbed/confined water relative to bulk water, were conducted on natural minerals or soils. In contrast, we chose to make some experiments on artificial "simple" material with size-controlled porosity.

In this paper, we present the isotopic fractionation between water adsorbed on porous silica tubes and water vapor at room temperature. The aim of this study is to follow

* Corresponding author. Fax: +33 169 154 917.
E-mail address: richard@geol.u-psud.fr (T. Richard).

0016-7037/$ - see front matter © 2006 Elsevier Inc. All rights reserved.
doi:10.1016/j.gca.2006.11.028

the variation of the isotopic D/H fractionation factor α with the relative humidity (RH), i.e., when the water films grow in the pores of the solid substrate. These α values at equilibrium between adsorbed water and vapor were compared to those between liquid and vapor at the same temperature. An approximate method derived from the Bigeleisen–Stern–Van Hook–Wolfsberg model (BSVHW; Stern et al., 1963) was used to account for the results and discuss the state of adsorbed/confined water in mesoporous media.

2. Experimental

2.1. Material

Full cylindrical porous silica tubes of 3 mm outer diameter, which are commonly used in liquid-phase chromatography, are used here as solid adsorbate. Measurements are all related to the same mass of adsorbate (452.68 mg), with a specific surface: $S_{BET} = 290.3 \pm 0.1\ m^2/g$. This surface was calculated with the BET model (Brunauer et al., 1938) from the N_2 adsorption isotherm performed with a COULTER SA 3100 and using the COULTER 2.13 software. The pore size distribution was also deduced from the N_2 adsorption experiment (Table 1).

Table 1
Pore size distribution deduced from N_2 desorption isotherm

Pore diameter range (nm)	Pore volume (μl/g)	Pore volume (%)
Under 6	15.41	1.56
6–8	60.98	6.19
8–10	120.07	12.19
10–12	233.57	23.7
12–16	407.88	41.39
16–20	99.51	10.10
20–80	35.89	3.64
Over 80	12.07	1.22
Total	985.38	100.00

2.2. Experimental protocol

An extraction line was built for this study (Fig. 1). Before each measurement, the line was evacuated to reach the initial vacuum condition (10^{-6} mbar). Valves 1, 2 and 3 (Fig. 1) were closed and liquid water was then introduced into the cell (reaction chamber) with a 5 μl SGE syringe with a precision of ±1%. The liquid vaporized because of the vacuum inside. The cell and the adsorbate container were isolated from each other, to avoid contaminations from one reservoir to another, and from the vacuum pump with valves (1, 2 and 3). This assures measuring the specific isotopic signal of vapor and adsorbed water. Water pressure was measured with an absolute pressure gauge (±0.1 mbar), and so the relation between the water volume introduced into the cell and the resulting vapor pressure was experimentally recorded (Section 3.2). The sample was put in contact with water vapor opening valve 2 over the time required to reach isotopic equilibrium, a time that is highly dependent on the water pressure (Fig. 2 and Section 3.1). To obtain the relative humidity (RH hereafter), the vapor pressure at equilibrium was divided by the saturated vapor pressure at the experimental temperature.

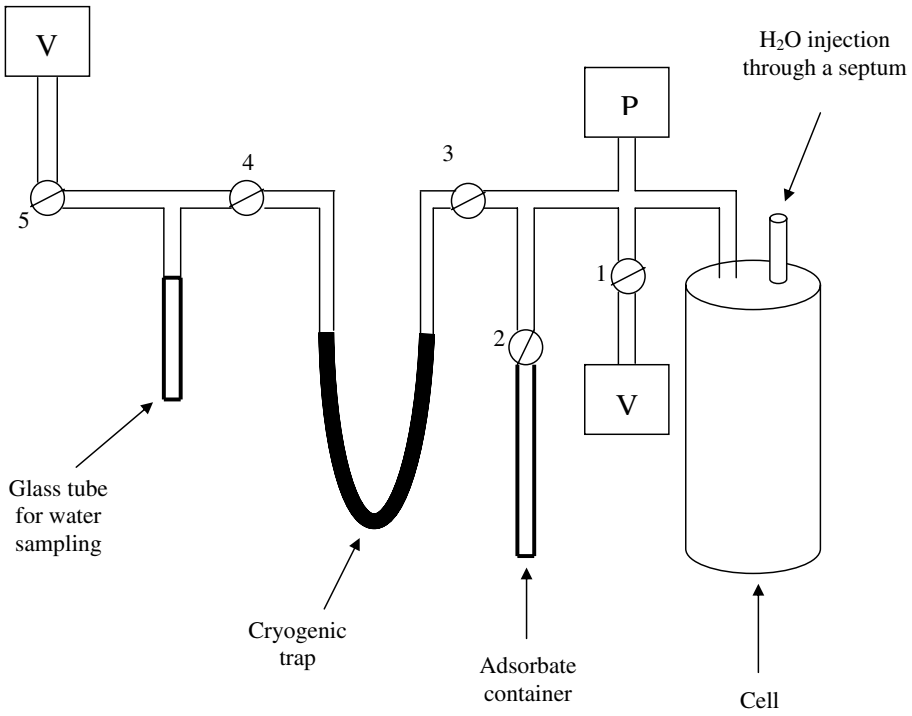

Fig. 1. Sketch of the extraction line, V stands for vacuum pump and P for pressure gauge. The numbers 1–5 refer to the position of valves.

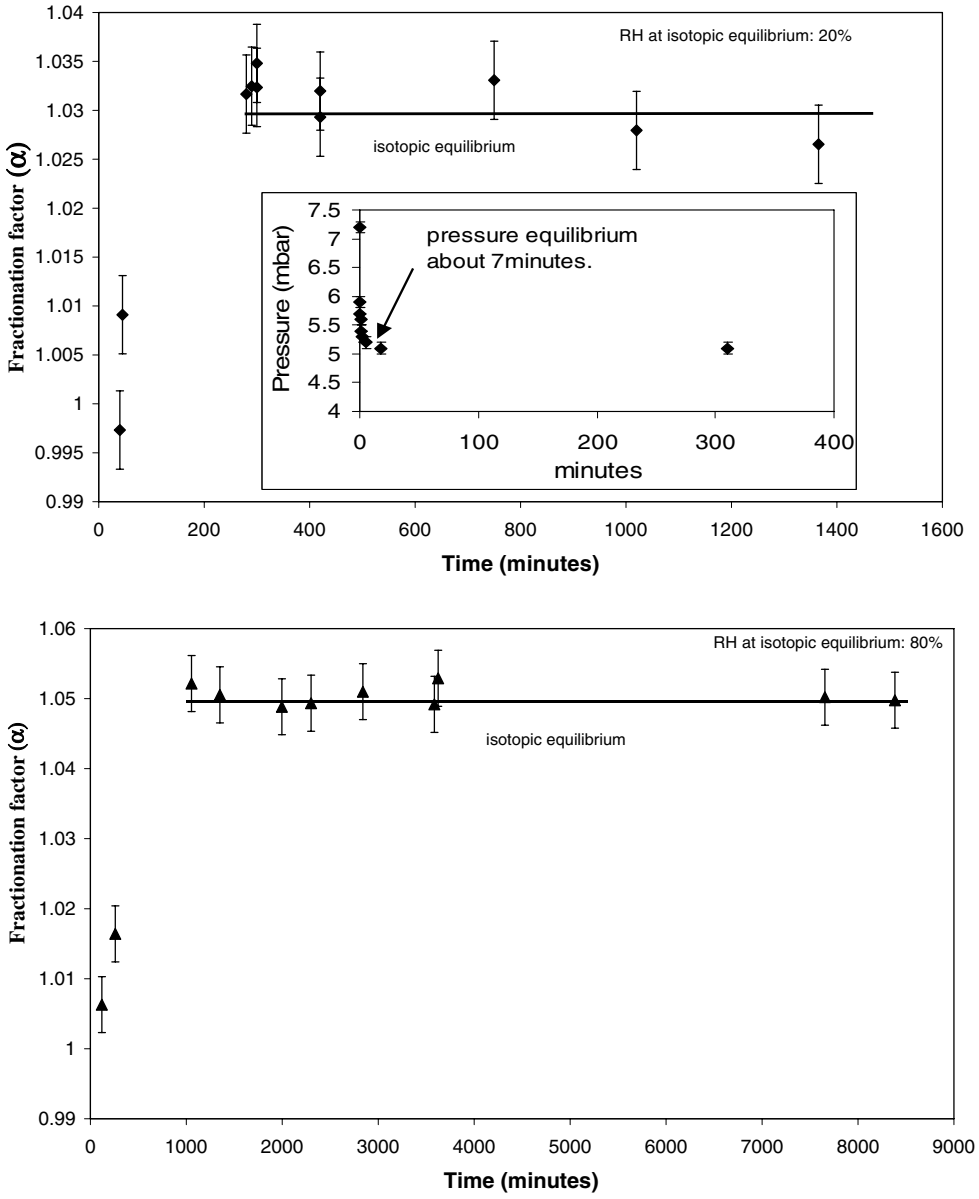

Fig. 2. Evolution of the fractionation factor α as a function of time for two different relative humidity (RH). Inset, the plot of the variation of the vapor pressure versus time (plateau = equilibrium pressure). Isotopes keep exchanging after reaching pressure equilibrium, thus the plateau is an equilibrium state.

Valve 4 was then closed, valves 1 and 2 being still closed, and water vapor was extracted with a cryogenic trap (liquid nitrogen, −196 °C). Additional pumping was performed to obtain a complete extraction. Thereafter, valves 3–5 were closed, prior to the evaporation of liquid water by heating to 360 °C, water vapor being released (opening valve 4) into the sampling glass tube (again with a cryogenic trap). Valve 4 was finally closed to finish sampling. The inner surface of the line (silica glass) where the equilibrium occurred is about 0.2 m^2. The adsorbed volume can be estimated from reliable adsorption isotherm of porous silica glass (e.g., Naono et al., 1979): 4 μmol was adsorbed at max on the inner walls, corresponding to 7.2×10^{-2} μl. As a consequence, the total quantity of water vapor and of water adsorbed on the silica tube adsorbates was always greater by several orders of magnitudes than the amount adsorbed on the inner surface of the line. Therefore, the isotopic exchange between the latter and water vapor is neglected hereafter.

To make sure that a complete water extraction from the silica tubes was achieved, the solid sample was subsequently heated to 450 °C in a furnace for 45 min, with additional vacuum pumping (15 min) and a liquid nitrogen trap. The collected water was trapped in the "U" tube and then released into the cell to measure its quantity. This water was further extracted with the initial procedure (used for vapor sampling) to analyse its isotopic composition. To evaluate the actual volume available to the water vapor inside the silica adsorbate container (cf. Fig. 1) the volume of the silica tubes (around 1.4×10^{-5} m^3) is subtracted from

Table 2
Experimental raw data and expected precisions

No.	P_i[a]	T[b]	P_{eq}[c]	P_{ad}[d]	Adsorbed[e]	RH_{eq}[f]	δ_{vap}[g]	δ_{ads}[g]	α[h]	t (min)
162	3.45 ± 0.1	293.15	2.5	0.95	3.0 ± 0.7	10.7 ± 0.5	−61	−29	1.035	645
163	3.6 ± 0.1	293.15	2.45	1.15	3.5 ± 0.7	10.5 ± 0.5	−60	−28	1.030	420
164	3.55 ± 0.1	292.65	2.55	1	3.1 ± 0.7	11.2 ± 0.5	−61	−21	1.043	720
167	3.55 ± 0.1	293.15	2.3	1.25	3.9 ± 0.7	9.8 ± 0.5	−58	−26	1.035	380
171	3.4 ± 0.1	292.15	2.5	0.9	2.9 ± 0.8	11.4 ± 0.5	−54	−30	1.026	295
115	5.6 ± 0.1	293.15	3.8	1.8	5.7 ± 0.9	16.2 ± 0.5	−63	−36	1.029	1140
189	5.9 ± 0.1	293.15	4	1.9	5.7 ± 0.9	17.1 ± 0.5	−57	−29	1.030	105
190	5.7 ± 0.1	292.15	3.8	1.9	5.9 ± 0.9	17.3 ± 0.6	−61	−26	1.037	720
113	6.9 ± 0.1	293.15	3.7	3.2	10.2 ± 0.8	15.8 ± 0.5	−60	−35	1.027	1365
114	7.1 ± 0.1	293.15	4.6	2.5	7.8 ± 0.9	19.7 ± 0.6	−62	−35	1.028	1020
124	7.3 ± 0.1	293.15	4.7	2.6	7.9 ± 0.9	20.1 ± 0.6	−61	−34	1.029	420
139	7 ± 0.1	292.15	4.7	2.3	7.2 ± 0.9	21.4 ± 0.6	−62	−32	1.032	420
145	7.3 ± 0.1	293.15	5	2.3	6.9 ± 0.9	21.4 ± 0.6	−59	−30	1.032	280
146	7.2 ± 0.1	293.15	5	2.2	6.7 ± 0.9	21.4 ± 0.6	−59	−28	1.032	290
149	7.1 ± 0.1	293.15	4.9	2.2	6.8 ± 0.9	20.9 ± 0.6	−57	−24	1.035	300
150	7.1 ± 0.1	292.15	4.7	2.4	7.5 ± 0.9	21.4 ± 0.6	−60	−29	1.033	750
151	7.25 ± 0.1	293.15	5.1	2.15	6.5 ± 0.9	21.8 ± 0.6	−57	−27	1.032	300
192	14.55 ± 0.1	294.15	9.95	4.6	13.9 ± 1.3	40.0 ± 0.6	−62	−28	1.036	600
194	14.3 ± 0.1	292.15	9.4	4.9	15.1 ± 1.2	42.8 ± 0.7	−61	−26	1.038	700
196	14.3 ± 0.1	293.15	9.7	4.6	14.2 ± 1.3	41.5 ± 0.7	−59	−27	1.034	765
197	14.4 ± 0.1	293.15	9.55	4.85	14.9 ± 1.2	40.8 ± 0.7	−63	−27	1.038	810
205	20.8 ± 0.1	293.15	13.4	7.4	23.5 ± 1.6	57.3 ± 0.8	−62	−28	1.036	685
206	20.5 ± 0.1	293.15	13	7.5	24.2 ± 1.6	55.6 ± 0.8	−62	−31	1.033	1180
207	20.9 ± 0.1	293.15	13.05	7.85	24.8 ± 1.6	55.8 ± 0.8	−62	−26	1.038	2490
265	20.5 ± 0.1	293.65	11.8	8.7	28.1 ± 1.6	48.9 ± 0.7	−63	−25	1.040	1090
218	28 ± 0.28	293.05	15.85	12.15 ± 0.38	38.3 ± 2.2	68.2 ± 0.9	−64	−24	1.043	5280
210	31.5 ± 0.32	294.05	17.5	14 ± 0.42	44.1 ± 2.4	70.8 ± 0.8	−65	−30	1.038	1110
212	31.5 ± 0.32	292.75	16.5	15 ± 0.42	47.3 ± 2.3	72.3 ± 0.9	−68	−24	1.047	2310
213	31.5 ± 0.32	292.55	17.15	14.35 ± 0.42	45.2 ± 2.4	76.1 ± 1.0	−65	−21	1.046	1090
214	31.5 ± 0.32	293.25	16.75	14.75 ± 0.42	46.5 ± 2.4	71.2 ± 0.8	−65	−23	1.045	1220
215	31.5 ± 0.32	293.55	16.7	14.8 ± 0.42	46.6 ± 2.4	71.4 ± 0.9	−64	−24	1.043	890
216	31.5 ± 0.32	293.55	17.5	14 ± 0.42	44.1 ± 2.4	73.0 ± 0.9	−67	−22	1.049	3725
217	31.5 ± 0.32	293.45	16.85	14.65 ± 0.42	46.1 ± 2.4	70.7 ± 0.9	−66	−23	1.046	3720
219	31.5 ± 0.32	293.05	16.55	14.95 ± 0.42	47.1 ± 2.4	71.2 ± 0.9	−66	−23	1.046	2480
220	31.5 ± 0.32	292.35	17.4	14.1 ± 0.42	44.4 ± 2.4	78.2 ± 1.0	−66	−26	1.043	15,390
263	31.5 ± 0.32	293.45	15.2	16.3 ± 0.42	51.3 ± 2.4	63.8 ± 0.8	−61	−20	1.044	2165
264	31.5 ± 0.32	293.25	16.8	14.7 ± 0.42	46.3 ± 2.4	71.4 ± 0.9	−62	−27	1.037	6560
260	31.5 ± 0.32	293.75	15.8	15.7 ± 0.42	49.4 ± 2.3	65.1 ± 0.8	−63	−20	1.046	2490
261	31.5 ± 0.32	293.15	16	15.5 ± 0.42	48.8 ± 2.3	68.4 ± 0.9	−64	−19	1.048	2295
221	38.5 ± 0.39	293.55	18.9	19.6 ± 0.49	61.7 ± 2.7	78.8 ± 0.9	−70	−23	1.050	7655
222	38.5 ± 0.39	293.15	19.3	19.2 ± 0.49	60.5 ± 2.7	82.5 ± 1.0	−70	−22	1.051	2840
223	38.5 ± 0.39	293.45	18.8	19.7 ± 0.49	62.1 ± 2.7	78.9 ± 0.9	−69	−20	1.052	1055
224	38.5 ± 0.39	292.45	18.7	19.8 ± 0.49	62.4 ± 2.7	79.9 ± 0.9	−70	−21	1.053	3625
225	38.5 ± 0.39	292.45	17.5	21 ± 0.49	66.2 ± 2.6	74.8 ± 0.9	−70	−23	1.051	1350
226	38.5 ± 0.39	292.95	18.1	20.4 ± 0.49	64.3 ± 2.7	78.3 ± 0.9	−69	−23	1.049	2300
227	38.5 ± 0.39	294.15	19	19.5 ± 0.49	61.4 ± 2.7	76.4 ± 0.9	−68	−22	1.049	3585
228	38.5 ± 0.39	293.85	19.3	19.2 ± 0.49	60.5 ± 2.7	79.0 ± 0.9	−68	−22	1.050	8385
229	38.5 ± 0.39	293.15	19	19.5 ± 0.49	61.4 ± 2.7	81.2 ± 0.9	−67	−22	1.049	1995
231	42 ± 0.42	293.25	20.15	21.85 ± 0.52	68.8 ± 2.9	85.6 ± 1.0	−69	−21	1.052	985
232	42 ± 0.42	294.15	19.3	22.7 ± 0.52	71.5 ± 2.9	77.6 ± 0.9	−71	−22	1.053	870
235	42 ± 0.42	294.15	18.2	23.8 ± 0.52	75.0 ± 2.8	73.1 ± 0.8	−72	−22	1.054	5405
236	42 ± 0.42	292.75	18.1	23.9 ± 0.52	75.3 ± 2.8	79.3 ± 1.0	−70	−22	1.051	2020
237	45.5 ± 0.42	293.15	17.5	28 ± 0.52	88.2 ± 2.7	74.8 ± 0.9	−68	−20	1.051	1457
238	45.5 ± 0.46	292.65	19	26.5 ± 0.56	83.5 ± 2.9	83.8 ± 1.0	−73	−21	1.056	3667
239	45.5 ± 0.46	293.15	19.1	26.4 ± 0.56	83.2 ± 3.0	81.7 ± 1.0	−73	−23	1.055	1440
240	45.5 ± 0.46	293.05	19.5	26 ± 0.56	81.9 ± 3.0	83.9 ± 1.0	−74	−20	1.058	2150
241	45.5 ± 0.46	293.75	18.5	27 ± 0.56	85.0 ± 2.9	76.2 ± 0.9	−73	−22	1.055	2370
242	45.5 ± 0.46	292.85	18.85	26.65 ± 0.56	84.0 ± 2.9	82.1 ± 1.0	−74	−24	1.053	2460
243	45.5 ± 0.46	292.45	17.8	27.7 ± 0.56	87.3 ± 2.9	79.5 ± 1.0	−70	−29	1.045	2220
244	45.5 ± 0.46	293.75	19.2	26.3 ± 0.56	82.8 ± 3.0	79.1 ± 0.9	−73	−25	1.052	2420
247	52.5 ± 0.46	293.45	18.65	33.85 ± 0.63	106.6 ± 3.1	78.3 ± 0.9	−74	−23	1.055	2295
249	52.5 ± 0.46	293.45	17.7	34.8 ± 0.63	109.6 ± 3.1	74.3 ± 0.9	−86	−38	1.053	5610

Table 2 (*continued*)

No.	P_i[a]	T[b]	P_{eq}[c]	P_{ad}[d]	Adsorbed[e]	RH_{eq}[f]	δ_{vap}[g]	δ_{ads}[g]	α[h]	t (min)
250	59.5 ± 0.46	294.15	19.2	40.3 ± 0.7	126.9 ± 3.4	77.2 ± 0.9	−81	−18	1.069	2860
251	59.5 ± 0.46	292.75	19.1	40.4 ± 0.7	127.3 ± 3.4	83.7 ± 1.0	−79	−29	1.054	3500
252	59.5 ± 0.46	292.15	18.5	41 ± 0.7	129.2 ± 3.4	84.2 ± 1.0	−79	−21	1.064	2610
255	59.5 ± 0.46	293.15	19.7	39.8 ± 0.7	125.4 ± 3.4	84.2 ± 1.0	−79	−26	1.057	2505
256	59.5 ± 0.46	292.15	19.2	40.3 ± 0.7	127.0 ± 3.4	87.3 ± 1.1	−81	−31	1.054	5370
259	59.5 ± 0.46	292.85	19	40.5 ± 0.7	127.6 ± 3.4	82.7 ± 1.0	−81	−30	1.056	3600

[a] Initial pressure in mbar with a ±0.1 precision gauge. Above $P°$, initial pressures are calculated from the relation between the volume injected and the corresponding pressure (Fig. 3).

[b] Room temperature in K when measuring the equilibrium pressure. The Hg thermometer gave a ±0.1° precision.

[c] Saturation pressure in mbar with the same precision as P_i, i.e., ±0.1.

[d] $P_{ad} = P_i - P_{eq}$ in mbar. Theoretical pressure of the adsorbed water if gaseous. Precision: $\Delta P_{ad} = \Delta P_i + \Delta P_{eq} = \pm 0.2$ mbar.

[e] Mass (mg) of adsorbed water per g of silica tube (mg_{water}/g_{silica}). First, adsorbed volume is deduced: $V_{ads} = V_i - V_{vap}$ with $V_{vap} = P_{eq}/0.7$ (Fig. 3). Then, $m = V_{ads} \times \rho / m_{silica}$. ρ from the currently recommended equation of state β. Error in ρ corresponds to a thermal deviation of ±0.1 °C, i.e., ±0.03 kg m^{-3}. Precision of m was calculated by derivation of this expression.

[f] $RH_{eq} = (P_{eq}/P°) \times 100$ is the relative humidity at the equilibrium pressure. $P°$ is calculated from Wagner and Pruß (2002) at the same temperature as P_{eq}. Error in $P°$ also corresponds to a variation of temperature of ±0.1 °C and is estimated to ±0.15 mbar.

[g] Fractionation data using the IRMS spectrometer with a ±2‰ precision.

[h] Fractionation factor calculated with δ values (see Section 2.3). The precision is ±0.004‰ and was obtained by a simple derivation of the relation between α and δ.

the total volume of the container. The vapor pressure measured during the experiments varied from 4 to 20 mbar, that is from 4×10^{-2} to 2×10^{-1} µl. Correspondingly, the adsorbed water volumes extracted from the silica tubes were 1.32–58 µl, respectively, i.e., they represent 3–0.3% of the sampled water and can be neglected hereafter.

The water samples were submitted to the standard reduction procedure with zinc (Coleman et al., 1982). We measured the δ values of the samples (Table 2) relative to the international standard V-SMOW. The values were determined with a mass spectrometer (dual inlet IRMS). The total reproducibility of the measurements is better than ±2‰. Potential fractionation within the extraction line has been checked by performing the described sampling procedure with standards and comparing the measured δ values with those obtained by direct isotopic analysis with the Zn reduction method. The results agree within 1.3‰, to be compared to the experimental precision (±2‰). Because of the low amount of extracted water, only deuterium analyses were performed (see Table 2).

The fractionation factor $\alpha_{\text{adsorbed water-vapor}}$ is defined as: $(1000 + \delta_{\text{adsorbed water}})/(1000 + \delta_{\text{vapor}})$, where δ are in [‰].

2.3. Extraction methods

The D/H ratio that could be measured according to the above protocol corresponds to a water volume ranging from 1 to 7 µl. When the water volume present in the vapor (remaining in the cell) and adsorbed (on the solid sample) phases exceeded 7 µl, the extraction became problematic since incomplete recovery can produce Rayleigh fractionation by distillation effect.

Three ways of extraction were tested (Table 3): by "direct sampling", by a "double sample carrier" (enabling to double the recoverable water volume), and by "equilibrium stages". Direct sampling was fully adapted when the water quantity in the cell was lower or equal to 7 µl. When it exceeded this value, the same direct method was still possible by successive sampling until removing the total amount of vapor (Table 3).

Whenever the amount of water in the cell exceeded 7 µl, another strategy than the successive sampling was used. It consists in introducing a piece of line with two glass tubes instead of one containing Zn between valves 4 and 5 (Fig. 1). In this way, it was possible to collect amounts of water up to 14 µl. As the whole amount was sampled in one extraction, no fractionation could occur. However, whenever the amount of water exceeded 14 µl, successive sampling was combined with this second method. The results agree with the other methods (Table 3).

For the third method, a large container was put between valves 4 and 5 to expand the vapor. Then, a part of the vapor volume was isolated in order to obtain a reduced sampling volume corresponding to 1–7 µl range of liquid water. This extraction avoided the distillation process (and fractionation) because, after expansion, the sampled vapor

Table 3
Comparison of the three sampling methods

Method	Injected volume (µl)	$\delta \pm 2$(‰)	Number of samples	Standard deviation
"Direct sampling"	45	−65	11	2
	55	−69	6	1
"Double sample carrier"	45	−66	11	2
"Equilibrium stage"	55	−68	2	0

was an aliquot fraction of the whole volume. Obviously, this was also the most time-consuming procedure.

The results obtained with the three methods are all in agreement (Table 3). Therefore, the direct sampling process was mostly used for practical reasons.

3. Results

3.1. Attainment of isotopic equilibrium

Prior to studying the measured fractionation factors, the attainment of isotopic equilibrium must be unambiguously proven. For a given value of RH the variations of equilibrium pressure and α were recorded as a function of time (Fig. 2). Despite thermal variations (20 ± 1 °C) that occurred during the experiment, an equilibrium plateau on the α vs time curve was systematically reached. The time needed to reach pressure equilibrium was shorter than the time needed to reach this isotopic plateau. For instance at 20% of RH (inset, Fig. 2a) the pressure equilibrium was reached in less than 10 min whereas the isotopic plateau was reached after 300 min. This time difference of the kinetics of isotopic and pressure equilibria suggests that the adsorbed phase exchanges with the vapor even

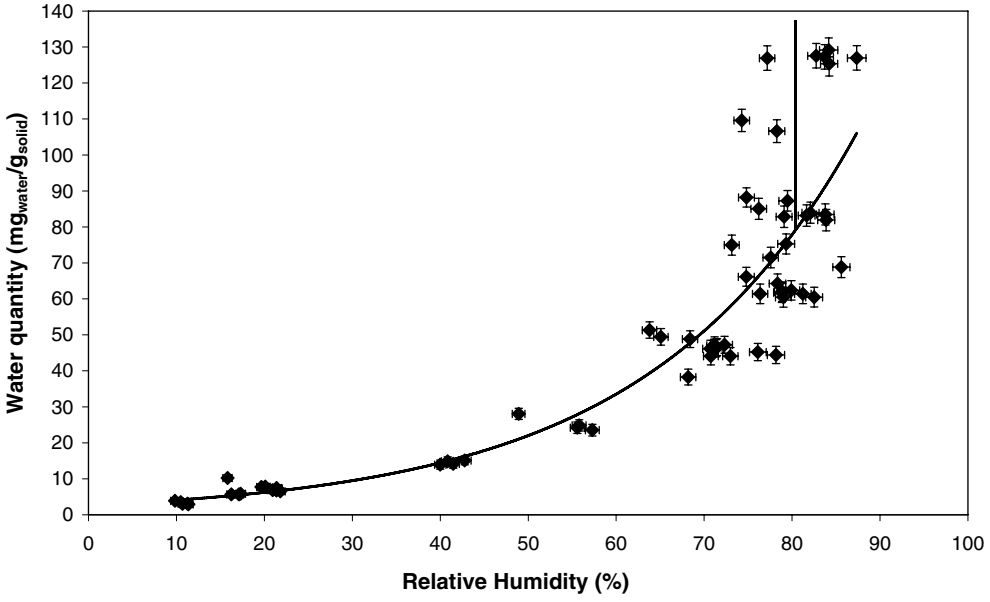

Fig. 3. Adsorption isotherm at 20 ± 1 °C of water adsorbed on porous silica tube. The exponential curve fits the data and the vertical line is only guide for eyes.

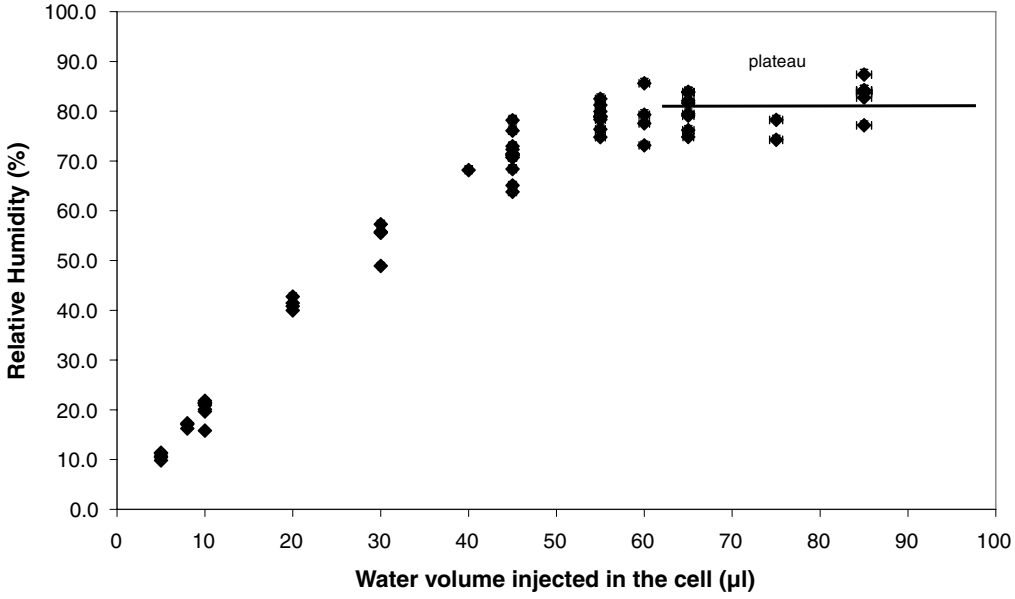

Fig. 4. Relative humidity (RH) at equilibrium as a function of the water volume injected into the cell. RH becomes constant at 80% illustrating the condensation into nano-pores. The horizontal line is a guide for eyes.

after pressure equilibrium. Thus, it is likely that the observed steady state (Fig. 2) corresponds to a true isotopic equilibrium.

3.2. Adsorption process

The volume of adsorbed water was calculated from the amounts of injected water and the water vapor. The adsorption isotherm displays the amount of adsorbed water (mg of water per g of solid) as a function of RH at 20 °C (Fig. 3). It follows an exponential function up to 80% of relative humidity. Beyond 80%, RH remains constant regardless of the volume of water injected into the cell (Fig. 4). It is noteworthy that this RH (80%) corresponds to the capillary condensation in 9.8 nm diameter pores (kelvin equation at zero contact angle), meaning that the saturated vapor pressure was attained for a large fraction of internal pores (44% of silica pores have diameters smaller than 12 nm; Table 1). In other words, at 80% RH, water vapor condensed in the nanopores, and RH remained constant until all the corresponding pore volume was filled.

The variation of the fractionation factor α with RH follows two linear trends with very different slopes (Fig. 5). For values of RH smaller than 60% α is almost constant (1.030 to 1.037 $\pm$ 0.004). Above 60% α has a much stronger dependence on RH (see Section 4.2).

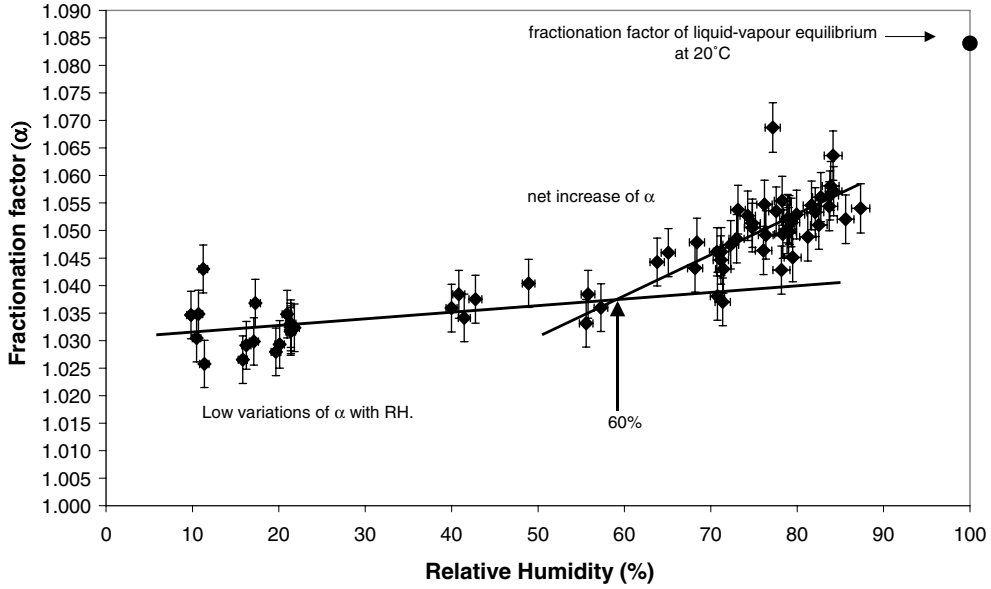

Fig. 5. Evolution of the fractionation factor (α) with increasing relative humidity (RH) in percent. Some points are outside the general trend, possibly due to thermal variation in the laboratory. Straight lines are guide for eyes.

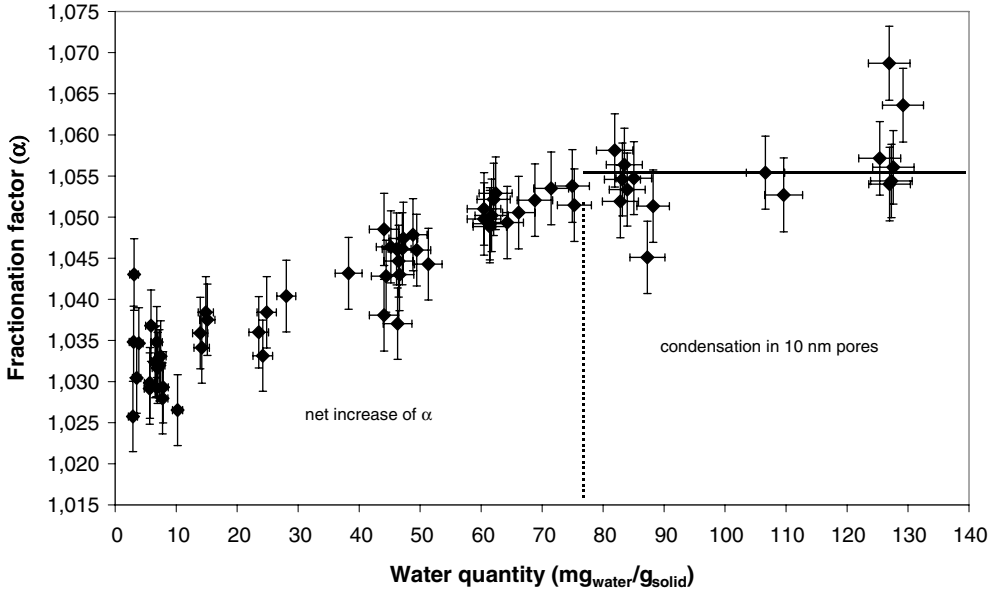

Fig. 6. Evolution of the fractionation factor as a function of the specific mass of adsorbed water (in mg/g) in the silica pores at equilibrium. Again, some points are outside the trend interpreted by temperature variations. The straight line is only a guide for eyes.

Plotting the α variation against the adsorbed water-specific mass (Fig. 6) shows that the adsorbed water quantity and α both increased until α became constant around 77 mg/g of adsorbed water (80% RH) (see also isotherm, Fig. 3). This demonstrates that the D/H ratio is a function of adsorbed water quantity. At 77 mg/g of adsorbed water α becomes nearly constant (Fig. 6) which corresponds to a vertical straight line (water condensation) on the adsorption isotherm (Fig. 3). The isotopic ratio remained constant while the water amount increased, meaning that there is no difference in the energetic status of the liquid water despite the occurrence of condensation. This is consistent with a condensation occurring in confined space by the collapse of two opposite thickening films. Liquid water changes from a true adsorbed situation (opposite two films) to a capillary bridge, probably affected by a confinement effect (see Section 4.2).

4. Discussion

4.1. Role of the zero-point energy

Basically, condensed phase isotope effect is due to the difference between the bond strengths formed by the light vs the heavier isotopes. Condensed phase of water is generally D-enriched compared to the vapor phase because of the better stability of the D bond. $\alpha_{\text{film–vapor}}$ greater than 1 means that film/confined water is D-enriched relative to vapor and that adsorbed/confined water is, isotopically speaking, a condensed "phase" (let us call it a phase for practical reason). The isotopic equilibrium between adsorbed water and vapor may be written as:

$$\mathrm{HOH_{ads}} + \mathrm{HOD_v} \leftrightarrows \mathrm{HOH_v} + \mathrm{HOD_{ads}} \tag{4.1}$$

The reactional coefficient is as follows:

$$K = \frac{(\mathrm{HOD})\mathrm{ads}(\mathrm{HOH})\mathrm{v}}{(\mathrm{HOH})\mathrm{ads}(\mathrm{HOD})\mathrm{v}} \approx \alpha = \frac{\left(\frac{\mathrm{D}}{\mathrm{H}}\right)_{\mathrm{ads}}}{\left(\frac{\mathrm{D}}{\mathrm{H}}\right)_{\mathrm{vap}}} \tag{4.2}$$

The liquid–vapor fractionation factor can be accurately calculated in the frame of the Bigeleisen–Stern–Van Hook–Wolfsberg model (BSVHW) (Stern et al., 1963), expressed by partition functions between the condensed phase and the vapor (Bigeleisen, 1963; Jansco and Van Hook, 1974). Actually, the isotopic effects in the water condensed phase result from an interplay between intramolecular (vibrational frequencies) and intermolecular (H-bonding) isotope effects. Among the whole vibration modes, the contribution of the stretching is five to six times greater than the others (see data from Majoube, 1971; Kakiuchi et al., 2001). Consequently, the OH-stretching behavior is considered relevant to account for the whole vibration behavior.

Within isothermal conditions at ambient temperature, the isotopic fractionation mostly depends on the zero-point energy (ZPE) difference between the O–H and O–D bonds (ΔZPE). For water, ZPE is the sum of the total internal vibrational ground state, that is:

$$\mathrm{ZPE} = \sum_{i=1}^{3} \frac{v_i}{2} \tag{4.3}$$

α relates to the ΔZPE difference:

$$[\Delta\mathrm{ZPE}_{\text{bulk liquid}} - \Delta\mathrm{ZPE}_{\text{vapor}}] \propto \alpha_{\text{liquid–vapor}} \tag{4.4}$$

From bulk to film, the present experiment shows that α is decreasing, meaning:

$$[\Delta\mathrm{ZPE}_{\text{bulk liquid}} - \Delta\mathrm{ZPE}_{\text{vapor}}] > [\Delta\mathrm{ZPE}_{\text{fim water}} - \Delta\mathrm{ZPE}_{\text{vapor}}] \tag{4.5}$$

There is no ZPE variation in the vapor phase so this inequality becomes:

$$[\Delta\mathrm{ZPE}_{\text{bulk liquid}}] > [\Delta\mathrm{ZPE}_{\text{film water}}] \tag{4.6}$$

The bending has a small dependence on H-bonding and is supposed to be constant. The latter inequality (Eq. (4.6)) can be translated in terms of the stretching mode vibration, what writes:

$$(\nu_{\mathrm{OH}} - \nu_{\mathrm{OD}})_{\text{bulk}} > (\nu_{\mathrm{OH}} - \nu_{\mathrm{OD}})_{\text{film}} \tag{4.7}$$

As a conclusion, the difference between ν_{OH} and ν_{OD} in the adsorbed water film should be smaller than in the liquid phase. The red shift of the intramolecular vibrations is known to be responsible of decreasing α (Jansco and Van Hook, 1974). Independent experiments pointed to a red shift of the OH-stretching band of water adsorbed onto oxide surfaces (Ershova et al., 1979; Foster and Ewing, 2000; Al-Abadleh and Grassian, 2003; Asay and Kim, 2005) and confined inside porous materials (e.g., Crupi et al., 2005; Richard et al., 2006). Therefore, with respect to the (4.7) inequality, ν_{OD} should follow the same decreasing trend, but with a smaller magnitude. Actually, the ratio of vibrational frequency between two isotopomers is known to be constant whatever the phase, around 1.36 for $\nu_{\mathrm{OH}}/\nu_{\mathrm{OD}}$ (Majoube, 1971). If ν_{OH} changes from 3404 $\mathrm{cm^{-1}}$ in the bulk to an average value of 3200 $\mathrm{cm^{-1}}$ in the film (Asay and Kim, 2005; Richard et al., 2006), ν_{OD} must change from 2500 $\mathrm{cm^{-1}}$ to around 2355 $\mathrm{cm^{-1}}$ (Table 4). As a consequence, OH ZPE is shifted by 100 $\mathrm{cm^{-1}}$ and that of OD by about 73 $\mathrm{cm^{-1}}$, what is consistent with the present explanation. Hence there is a "compression" of the ΔZPE at the bulk liquid → adsorbed/confined liquid transition. A sketch of the H_2O/HOD potential can be drawn (Fig. 7, Table 4).

4.2. Water state as a function of RH

The slope change of α(RH) may be related to a change in the molecular water dynamics from a 2-D behavior (below 60%) to a 3-D behavior (above 60%). The 2-D behavior defines a regime dominated by the dynamics of the O–H(O–D) bond itself, that is by the intramolecular vibration. Otherwise speaking, the constancy of α(RH) indicates that there is not any significant vibrational change through the RH range: each adsorbed water molecule vibrates in the same way as the others, with possible lateral

Table 4
IR frequencies of water in the gas (upper part), liquid (middle part) and adsorbed (lower part) phases with the associated ZPE of water

Frequencies (cm^{-1})	$H_2{}^{16}O$ (cm^{-1}) ($\Delta v/\Delta T$)	ZPE[c]	$HD^{16}O$ (cm^{-1})	ZPE[c]	ΔZPE
v_1	3657[a]	4503.8	2726.7[a]	3918.2	585.6
v_2	1594.6[a]		1402.2[a]		
v_3	3756[a]		3707.5[a]		
v_{OH-OD}	3404 (0.7)[a,b]	4225.5	2500 (0.5)[a,b]	3223.4	1002.1
v_2	1643 (−0.1)[a,b]		1446.8 (−0.06)[a,b]		
v_L	440 (−0.7)[a]	No	345 (0.7)[a]	No	No
	576 (−0.7)[a]		475.2 (0.7)[a]		
	475.2 (−0.7)[a]		776.4 (0.7)[a]		
v_T	171 (−0.2)[a,b]	No	167.9 (−0.2)[a]	No	No
v_{OH-OD}	3200	4021.5	2355	3078.4	943.1
v_2	1643 (−0.1)[a,b]		1446.8 (−0.06)[a,b]		

v_1, v_3, and v_2 are, respectively, the symmetric and asymmetric OH-stretching and -bending modes of water. v_{OH-OD} are the uncoupled OH and OD vibrations. v_L and v_T are the hindered rotations (libration) and translations.
$\Delta ZPE = ZPE_{HOH} - ZPE_{HOD}$.
[a] Majoube (1971).
[b] Eisenberg and Kauzmann (1969).
[c] Water ZPE is calculated according to Eq. (4.3): $ZPE = (v_1 + v_2 + v_3)/2$, as $(v_1 + v_3)/2 = v_{OH}$, $ZPE = v_{OH} + v_2/2$.

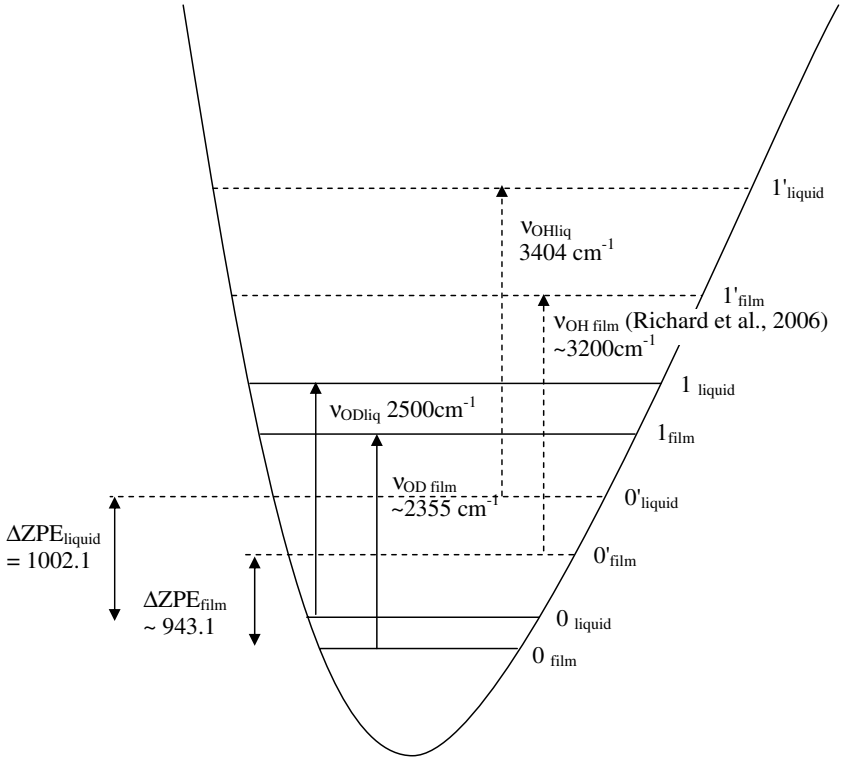

Fig. 7. Idealized scheme of the H–O–H and H–O–D potential. 0 and 0′ are the ground-state energies of H–O–D and H–O–H, respectively; 1 and 1′ are the corresponding excited levels reached at stretching excitation. Stronger H-bond of adsorbed "phase" involves lower transition energy and thus decreases the ΔZPE difference between H–O–H and H–O–D. v_{OH} of film water is deduced from observations and the corresponding v_{OD} is estimated by the constant isotopic ratio between v_{OH} and v_{OD} (see text).

coupling. The 3-D regime might be related to the occurrence of intermolecular dynamics: the vibration now depends on the state and the extension of the H-bond network. Obviously, the H-bond network depends on the molecular quantity and on the occurrence of poly-molecular stacking of water.

This transition has been already recorded with other techniques. Two-dimensional ice-like water monolayer was infraredly detected on calcite surfaces below 50% RH, which evolved to three-dimensional water-like layer above this RH value (Al-Hosney and Grassian, 2005). Meanwhile, Kendall and Martin (2005) proposed the conversion of 2-D water layer to a 3-D structure at 55% RH on calcite surfaces, based on scanning polarization microscopy data. A third approach coupling atomic force microscopy and ion scattering spectroscopy (Hausner et al., 2007) plot-

ted the transition from a two- to three-dimensional structure of the hydrating water film (also on calcite surfaces) at around 45% RH. Our isotopic experiment shows consistent results in spite of using a different solid surface.

At higher RH (80%), the liquid–vapor fractionation factor of water capillary condensed in 10 nm pore is recorded (plateau on Fig. 6). It is lower than that between bulk liquid water and vapor phase. Yet, capillary water is usually bulk liquid, and therefore its properties can be predicted from an equation of state as a function of decreasing water pressure (Mercury and Tardy, 2001; Mercury et al., 2003), which should not imply a measurable isotopic fractionation relative to bulk liquid. From these considerations, it can be deduced that capillary water in these nano-pores is confined (at least slightly), i.e., affected by the proximity of the pore walls. Generally speaking, the geometrical frustration is known to induce some changes on dynamical and static properties (e.g Takamuku et al., 1997; Benesi et al., 2004). From the present experiments, $\alpha_{film-vapor}$ is always lower than $\alpha_{liquid-vapor}$ (1.085 at 20 °C; Majoube, 1971) and increased at max. to 1.055 ± 0.004 (nano-pores condensation). Thus, porous confinement (solid–liquid–solid interactions) isotopically acts as the surface confinement (solid–liquid–air interactions) does. In other words, adsorption and confinement between solids both reduce the liquid–vapor fractionation factor, and are isotopically analogous. Infrared spectroscopic experiments also showed that adsorbed and confined water both exhibit the same trend of vibrational frequencies, with a red shift of the OH-stretching band relative to the bulk (e.g., Richard et al., 2006).

5. Conclusion

The deuterium fractionation factor between adsorbed/confined water on porous silica tubes and vapor is lower than the one between liquid and vapor at ambient temperature, evidencing that water films have specific properties deviating from the bulk liquid ones. Another interesting fact is the lower capillary water-vapor fractionation factor relative to the bulk-vapor one, which tends to indicate that the fractionation factor is very sensitive to confinement effect. By the way, this result seems to contradict the common opinion that surface forces do not affect the confined liquid beyond about 1.5 nm from the solid (Michot et al., 2002).

Interestingly, the fractionation factor appears sensitive to the surface water dynamics with two regimes distinguished by their α(RH) behaviour. Such transition from a 2-D to 3-D behavior has been already pointed out on calcite surfaces, making the surface ions mobiles (Kendall and Martin, 2005) and leading to some surface restructuring due to dissolution-reprecipitation events (Hausner et al., 2007). Therefore, this change of dimensionality is of geochemical significance and makes the water layer able to weather the solid surface. The fractionation factor could be a probe of this chemical "activation".

The present study also gives some indications about the composition of bound water in the geological "nanoporous" formations. Adsorbed water, that is water film deposited onto a solid surface open to the air, displays the same trend as water held in narrow channels. In the argillaceous formations, a very significant part of porosity corresponds to pore sizes smaller than 10–15 nm. It is very likely that bound water in these rocks is depleted in deuterium with respect to "free" water, what is consistent with literature (Stewart, 1972; Araguás-Araguás et al., 1995; Karlsson, 2001). This has to be confirmed by doing the same type of experiments on natural rock or mineral samples.

A further quantitative step will be to calculate the partition function of the condensed adsorbed phase, to deduce the thermodynamic potential of the adsorbed film. Additionally, we can deduce stretching frequencies from this partition function and compare them to the IR records to definitely and quantitatively test the consistency of the whole reasoning. Due to the strong energetic similarity between adsorbed and confined states, these calculations should open a way to quantitatively treat the solid–solutions interactions in the confined/adsorbed regime.

Acknowledgments

The porous silica sample was graciously supplied by Professor Satoru Nakashima, formerly at the Tokyo Institute of Technology, Interactive Research Center of Science, now at Osaka University, Department of Earth and Space Science. BET measurements were done by Sylvain Bassot at the Institut de Radioprotection et de Sureté Nucléaire, DPRE/SERGD in Fontenay-aux-Roses. Critical reviews and readings of G. Koehler, H. Zeyen, J. Teixeira, R. Reeder, and two anonymous reviewers considerably improved the scientific content and the English writing of the manuscript. Two critical reviews, large editing work, and constant assistance of J. Horita are gratefully acknowledged.

Associate editor: Juske Horita

References

Al-Abadleh, H.A., Grassian, V.H., 2003. FT-IR study of water adsorption on aluminum oxide surfaces. *Langmuir* **19**, 341–347.

Al-Hosney, H.A., Grassian, V.H., 2005. Water, sulphur dioxide and nitric acid adsorption on calcium carbonate: a transmission and ATR-FTIR study. *Phys. Chem. Chem. Phys.* **7**, 1266–1276.

Araguás-Araguás, L., Rozanski, K., Gonfiantini, R., Louvat, D., 1995. Isotope effects accompanying vacuum extraction of soil water for stable isotope analyses. *J. Hydrol.* **168**, 159–171.

Asay, D.B., Kim, S.H., 2005. Evolution of the adsorbed water layer structure on silicon oxide at room temperature. *J. Phys. Chem. B* **109**, 16760–16763.

Benavente, D., Garcia del Cura, M.A., Garcia-Guinea, J., Sanchez-Moral, S., Ordonez, S., 2004. Role of pore structure in salt crystallization in unsaturated porous stone. *J. Cryst. Growth* **260**, 532–544.

Benesi, A.J., Grutzeck, M.W., O'Hare, B., et Phair, J.W., 2004. Room temperature solid surface water with tetrahedral jumps of ^2H nuclei detected in ^2H_2O-hydrated porous silicates. *J. Phys. Chem. B* **108**, 17790–17793.

Bigeleisen, J., 1963. Quantum effects in liquid hydrogen. *J. Chem. Phys.* **39**, 769–777.

Bogdan, A., 2002. Phase transitions in finely divided aqueous systems. In: Somasundara, P. (Ed.), *Encyclopedia of Surface and Colloid Science*. Marcel Dekker, New York, pp. 4002–4016.

Boisson, J.Y., Bertrand, L., Heitz, J.F., Moreau-Le-Golvan, Y., 2001. In situ and laboratory investigations of fluid flow through an argillaceous formation at different scales of space and time, Tournemire tunnel, southern France. *Hydrogeol. J.* **9** (1), 108–123.

Brunauer, S., Emmet, P.H., Teller, E., 1938. Adsorption of gases in multimolecular layers. *J. Am. Chem. Soc.* **60**, 309–319.

Coleman, M.L., Shephred, T.J., Rousse, T.E., Moore, G.R., 1982. Reduction of water with zinc for hydrogen isotope analysis. *Anal. Chem.* **54**, 993–995.

Crupi, V., Majolino, D., Migliardo, P., Venuti, V., 2005. Dynamical properties of liquids in restricted geometries. *J. Mol. Liq.* **117**, 165–171.

Eisenberg, D., Kauzmann, W., 1969. *The Structure and Properties of Water*. Oxford, New York.

Ershova, G.F., Zorin, Z.M., Churaev, N.V., 1979. Infrared absorption spectra of polymolecular adsorbed layers of water on quartz surface. *Colloid J. USSR* **41** (1), 13–16.

Foster, M.C., Ewing, G.E., 2000. Adsorption of water on the NaCl (001) surface. II. An infrared study at ambient temperatures. *J. Chem. Phys.* **112** (15), 6817–6826.

Hausner, D.B., Reeder, R.J., Strongin, D.R., 2007. Humidity-induced restructuring of the calcite surface and the effect of divalent heavy metals. *J. Colloid Interf. Sci.* **305**, 101–110.

Hendry, M.J., Kellna, C.J., Wassenaar, L.I., Shaw, J., 2004. Characterizing the hydrogeology of a complex clay-rich aquitard system using detailed vertical profiles of the stable isotopes of water. *J. Hydrol.* **293**, 47–56.

Jansco, G., Van Hook, W.A., 1974. Condensed phase isotope effects (especially vapor pressure isotope effects). *Chem. Rev.* **74**, 689–744.

Kakiuchi, M., Abe, T., Nakayama, H., 2001. D/H fractionation factor between water vapor and crystal water of copper chloride dihydrate: statistical mechanical approach based on raman spectra. *Geochem. J.* **35**, 285–293.

Karlsson, H.R., 2001. Isotope geochemistry of zeolites. In: *Natural Zeolites: Occurrence, Properties, Application. Reviews in Mineralogy and Geochemistry*, vol. 45, Chapter 4. Mineralogical Society of America, pp. 163, 666pp.

Kendall, T.A., Martin, S.T., 2005. Mobile ions on carbonate surfaces. *Geochim. Cosmochim. Acta* **69**, 3257–3263.

Majoube, M., 1971. Fractionnement en oxygène 18 et en deutérium entre l'eau et sa vapeur. *J. Chim. Phys.* **68**, 1423–1436.

Mercury, L., Tardy, Y., 2001. Negative pressure of stretched liquid water. Geochemistry of soil capillaries. *Geochim. Cosmochim. Acta* **65**, 3391–3408.

Mercury, L., Azaroual, M., Zeyen, H., Tardy, Y., 2003. Thermodynamic properties of solutions in metastable systems under negative or positive pressures. *Geochim. Cosmochim. Acta* **67**, 1769–1785.

Michot, L.J., Villiéras, F., Francois, M., Bihannic, I., Pelletier, M., Cases, J-M., 2002. Water organisation at the solid–aqueous solution interface. *C. R. Geosci.* **334**, 1–21.

Naono, H., Fujiwara, R., Yagi, M., 1979. Determination of physisorbed and chemisorbed waters on silica gel and porous silica glass by means of desorption isotherms of water vapor. *J. Colloid Interf. Sci.* **76**, 75–82.

Patriarche, D., Ledoux, E., Michelot, J.-L., Simon-Coinçon, R., Savoye, S., 2004. Diffusion as the main process for mass transport in very low water content argilites: 2. Fluid low and mass transport modeling. *Water Resources Res.* **40** (W01517). doi:10.1029/2003WR0022700.

Richard, T., Mercury, L., Poulet, F., d'Hendecourt, L., 2006. Diffuse Reflectance Infrared Fourier Transform Spectroscopy as a tool to detect the water state in mineral powders. *J. Colloid Interf. Sci.* **304** (1), 125–136.

Rübel, A., Bath, A., 2002. Pore water extraction by vacuum distillation and diffusive equilibration for oxygen and hydrogen stable isotopic analyses. In: Pearson, F.J. et al. (Eds.), *Geochemistry of Water in the Opalinus Clay Formation at the Mont Terri Rock Laboratory* . Mont Terri Project Tech. Rep. 2003-03 (Annex). *Geology Series*, FOWG Bern, A4-1/A4-11.

Rübel, A.P., Sonntag, C., Lippmann, J., Pearson, F.J., Gautschi, A., 2002. Solute transport in formations of very low permeability: profiles of stable isotope and dissolved gas contents of pore water in the Opalinus Clay. Mont Terri, Switzerland. *Geochim. Cosmochim. Acta* **66**, 1311–1321.

Santiso, E.E., George, A.M., Heath Turner, C., Kostov, M.K., Gubbins, K.E., Buongiorno-Nardelli, M., Sliwinska-Bartkowiak, M., 2005. Adsorption and catalysis: the effect of confinement on chemical reactions. *Appl. Surf. Sci.* **252**, 766–777.

Seshadri, K., Wilder, J.W., Smith, D.H., 2001. Measurements of equilibrium pressures and temperatures for propane hydrate in silica gels with different pore-size distributions. *J. Phys. Chem. B* **105**, 2627–2631.

Shirinyan, A.S., Gusak, A.M., Wautelet, M., 2005. Phase diagram versus diagram of solubility: what is the difference for nanosystems? *Acta Mater.* **53**, 5025–5032.

Stern, M.J., Van Hook, W.A., Wolfsberg, M., 1963. Isotope effects on internal frequencies in the condensed phase resulting from interaction with the hindered translations and rotations. The vapor pressure of the isotopic ethylenes. *J. Chem. Phys.* **39**, 3179–3195.

Stewart, G.L., 1972. Clay-water interaction, the behavior of ^{3}H and ^{2}H in adsorbed water, and the isotope effect. *Soil Sci. Soc. Am. Proc.* **36**, 421–426.

Takamuku, T., Yamagami, M., Wakita, H., Masuda, Y., Yamaguchi, T., 1997. Thermal property, structure, and dynamics of supercooled water in porous silica by calorimetry, neutron scattering, and NMR relaxation. *J. Phys. Chem. B* **101**, 5730–5739.

Uchida, T., Ebinuma, T., Takeya, S., Nagao, J., Narita, H., 2002. Effects of pore sizes on dissociation temperatures and pressures of methane, carbon dioxide, and propane hydrates in porous media. *J. Phys. Chem. B* **106**, 820–826.

Wagner, W., Pruß, A., 2002. The IAPWS formulation 1995 for the thermodynamic properties of ordinary substance for general and scientific use. *J. Phys. Chem. Data* **31**, 387–535.